Astron. Astrophys. 80, 201–211 (1979)

ASTRONOMY
AND
ASTROPHYSICS

The Radio Properties of the X-ray Cluster Abell 2256

A. H. Bridle[1], E. B. Fomalont[2], G. K. Miley[3], and E. A. Valentijn[3]

[1] Queen's University at Kingston, Ontario, Canada K7L 3N6
[2] National Radio Astronomy Observatory, Green Bank, West Virginia 24944, USA
[3] Sterrewacht, Huygens Laboratorium, Leiden, The Netherlands

Received March 13, 1979

Summary. The complex radio emission from the X-ray cluster Abell 2256 has been mapped using the WSRT at 1415 MHz with a resolution of 23″. The cluster contains: 1. at least four and possibly eight radio galaxies with head-tail morphology; 2. a 4′ radio source with an unusually steep spectrum ($\alpha \sim 1.7$) and a unique morphology; 3. emission extending over a 1×0.3 Mpc area with a remarkably uniform 610-to-1415 MHz spectral index of 0.8 ± 0.1, about 20% linear polarization, and a relatively uniform magnetic field.

The ~10′ diffuse emission reported at 610 MHz by Bridle and Fomalont (1976) was at our detection limit at 1415 MHz and comparison of the 151-MHz map of the cluster by Masson and Mayer (1978) with the WSRT maps suggests that this emission has a relatively steep spectrum. The "excess" emission at frequencies below 80 MHz may arise from this diffuse component as well as from the more compact steep-spectrum component described above.

The bivariate radio luminosity function in the cluster does not differ significantly from that of field ellipticals, suggesting that the complexity of radio morphology in the cluster is due more to the intracluster environment in Abell 2256 than to unusual properties of the individual galaxies. The powerful X-ray emission associated with Abell 2256 and the relatively large velocity dispersion of the cluster galaxies support this view.

Some physical parameters are derived for the radio sources in Abell 2256 and it is shown that all the observed radio emission could readily be confined by the hot gas needed if the observed X-rays are emitted by thermal bremsstrahlung. The mechanism of the X-ray luminosity in this cluster is uncertain however, in the absence of an accurate X-ray position and morphology for comparison with our data.

Key words: clusters of galaxies – head-tail radio sources – cluster X-ray sources – radio spectra – radio polarization

Introduction

Abell 2256 is one of the most powerful cluster X-ray sources (3U 1707+78) and its radial velocity dispersion is among the largest observed for any cluster (Faber and Dressler, 1977). The 610-MHz emission from Abell 2256 was shown by Bridle and Fomalont (1976, Paper I) to be remarkably complex: five discrete sources, three of which had slightly-resolved head-tail structures, were identified with cluster galaxies, and two diffuse emission regions (each of largest linear extent about 1 Mpc) were found near the cluster centre. The integrated emission from the cluster has a steep spectrum ($\alpha \sim 1.9$) between 22.25 and 81.5 MHz (Costain et al., 1972) and the X-ray emission is extended by ~16′ (Kellogg and Murray, 1974). Such associations between steep-spectrum decametric sources and extended X-ray sources are common in rich clusters and two mechanisms have been proposed to explain them.

In the thermal-bremsstrahlung model which is favoured by recent X-ray spectral-line observations (Serlemitsos et al., 1977), a hot dense intracluster medium produces the X-rays and also prolongs confinement of the radio emission from galaxies in the cluster, allowing synchrotron losses to produce localised steep-spectrum sources before they are quenched by adiabatic expansion (Baldwin and Scott, 1973). In the inverse Compton model a large volume of the cluster is filled with relativistic electrons having a steep power-law energy distribution; the lower-energy electrons produce X-rays by inverse Compton scattering on the 3-deg background radiation, while higher-energy electrons produce an extended diffuse steep-spectrum radio source by synchrotron radiation in an extensive weak intergalactic magnetic field.

We have mapped Abell 2256 using the Westerbork Synthesis Radio Telescope (WSRT) at 1415 MHz. The observations, made with more than twice the resolution in Paper I, were designed to investigate further the structure of the cluster radio galaxies and to examine the distribution of the 610–1415 MHz spectral index across the complex emission by comparison with the earlier 610 MHz results. Our purpose has been to study the processes of particle injection and confinement in the cluster, as indicated by the morphology, spectrum and polarization of the complex radio emission.

Throughout this paper we assume Abell 2256 to be at a distance of 340 Mpc [$\bar{z} = 0.0566$ (Paper I) and $H_0 = 50\,\mathrm{km\,s^{-1}\,Mpc^{-1}}$].

I. The Radio Maps

Both the total intensity and linearly polarized intensity were mapped at 1415 MHz. Relevant parameters of the observing session at 1415 MHz and of the previous session at 610 MHz (Paper I) are shown in Table 1. The calibration and mapping of the data were performed in the usual manner (Brouw, 1971; Högbom and Brouw, 1974) and the effects of the grating lobes of strong sources in the field were removed either by subtracting the contribution of the strongest unresolved sources from the

Send offprint requests to: A. H. Bridle

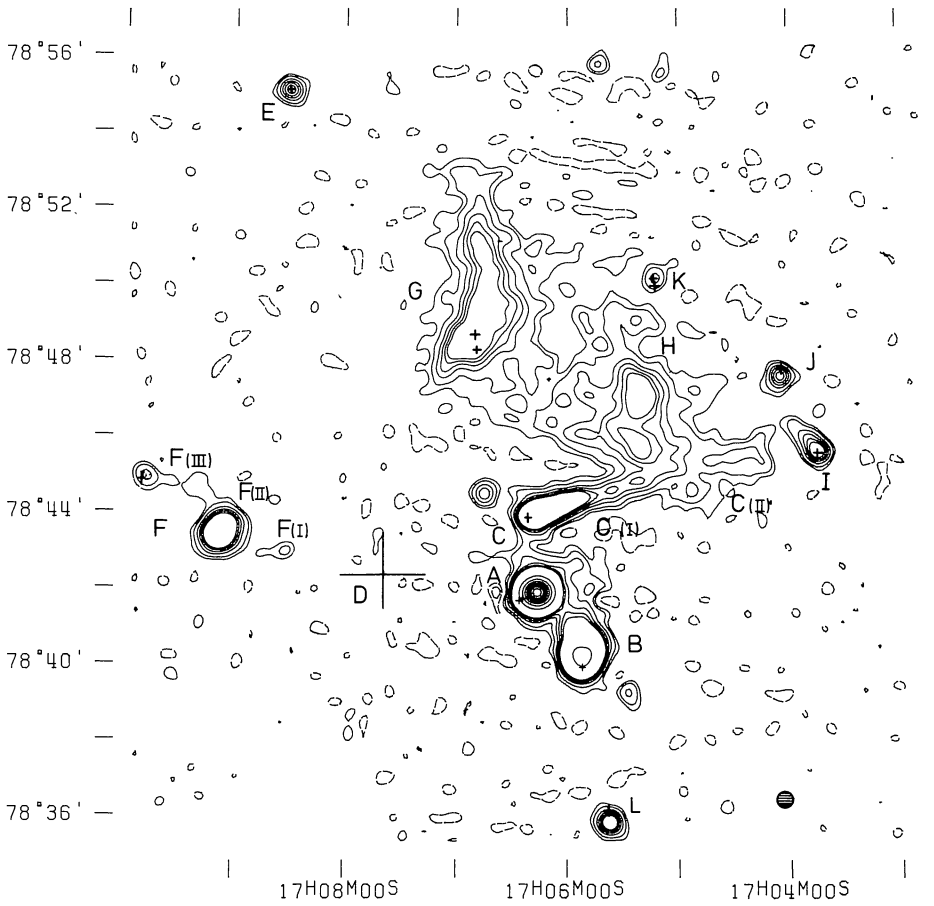

Fig. 1. Radio map of Abell 2256 at 1415 MHz with 23″ resolution. Contour levels are 0.5, 1, 2, 3, 4, 5 and from 30 to 205 mJy in intervals of 25 mJy per synthesized beam area. Continuous contours indicate positive levels and dashed contours negative levels. The shaded ellipse (bottom right) shows the half-power synthesized beam. Small crosses mark the positions of some cluster galaxies possibly associated with the radio emission. The large cross indicates the position at which point source *D* (max contour level 11) was subtracted from the map. Letter designations are shown for the major components

Table 1. Parameters of the Observations and Maps of Abell 2256

Frequency (MHz)	1415	610
Observing time (h)	4 x 12	2 x 12
Observing period	12 Aug.-8 Sept., 1975	27 Jan.-1 April, 1975
Field center - r.a. (1950)	$17^h06^m22^s$	$17^h06^m22^s$
- dec (1950)	78°45'48"	78°45'48"
Primary beam size (HPBW) (arc min)	36 x 37	84 x 85

	1415 MHz		610 MHz	
	Fig. 1	Fig. 2a	Paper I	Fig. 2b
Min. spacing (m)	36	36	36	72
Max. spacing (m)	1452	630	1440	1440
Incremental spacing (m)	18	18	36	36
25% grading at (m)	1404	629	1440	1440
Array size	512x512	512x512	512x512	512x512
Separation between array points (arc sec)	9x9	21x22	21x22	21x22
Point sources subtracted	13	0	20	20
Radius of first grating ring (arc min)	40x41	40x41	47x48	47x48
Restoring HPBW (arc sec)	23x23	55x56	55x56	55x56
R.m.s. noise (mJy)	0.4	0.6	1.0	1.0

Table 2. Observed parameters for the major components in Abell 2256

Comp.	Position (1950) R.A.	Position (1950) Dec.	Flux Density 610 MHz	Flux Density 1415 MHz	Spectral Index	Angular Extent size (arcsec)	Angular Extent p.a. (deg)	Optical Galaxy Position (1950) R.A.	Optical Galaxy Position (1950) Dec.	m_p
A	$17^h06^m18^s$	78°41'57"	327 ±17	157 ±10	0.87±0.10	15x 5	110	$06^m19^s.34$	41'53".4	16.6
B	17 05 52	78 40 40	117 ± 7	62 ± 4	0.75±0.10	120x 40	10	05 51.70	39 55.6	16.5
C(i)	17 06 00	78 44 00	88 ± 6	39 ± 3	0.97±0.12	90x 50	110	06 21.02	43 52.6	16.7
C(ii)	17 05 00	78 45 00	114 ± 8	48 ± 8	1.04±0.13	300x 50	110			
D	17 07 38.46±0.07	78 42 22.2±0".2	19.3± 1.5	11.0± 1.2	0.67±0.16	<5		07 38.84	42 21.9	16.2
D(Diff.)	17 08	78 42	100			∿ 600				
E	17 08 30.6 ±0.2	78 55 06.6±0.4	8 ± 2	4.4± 1.0	0.73±0.40	<5		08 30.84	55 06.5	16.8
F(i)	17 08 31.7 ±0.4	78 42 59.5±1.1	23 ± 3	6.4± 1.3	1.5 ±0.3	40x<15	90			
F(ii)	17 09 07.2 ±0.4	78 43 24.6±2	97 ± 6	22 ± 2	1.7 ±0.1	45x 45				
F(iii)	17 09 47.0 ±0.3	78 44 54.8±0.6	43 ± 4	11 ± 2	1.6 ±0.4	30x<15	90	09 48.81	44 53.1	16.7
G	17 06 45	78 50 00	348 ±26	185 ±13	0.75±0.12	100x 50	0			
H	17 05 20	78 47 00	323 ±23	166 ±11	0.79±0.11	240x100	0			
I	17 03 45	78 45 42	25 ± 2	10.0± 1.2	1.11±0.14	100x<15	45	03 42.95	45 30.4	17.0
J	17 04 04.2 0.2	78 47 34.1±0.4	14 ± 2	6.5± 1.1	0.89±0.26	<5		04 02.73	47 43.2	16.7
K	17 05 12.0 0.3	78 50 10.0±0.6	14 ± 2	5.2± 1.0	1.16±0.28	<5		05 12.06	50 06.1	17.0
L	17 05 37.1 0.2	78 35 51.1±0.3	11 ± 2	5.1± 1.0	0.92±0.32	<5		05 37.76	36 11.5	19.0
M	17 12 25	78 45 20	23 ± 5	12 ± 3	0.77±0.2	56x<15	5	12 17.9	45 51	17.7

visibility data before mapping or by use of the CLEAN deconvolution technique developed by Högbom (1974). All maps were corrected for the effects of the primary beam attenuation.

At each frequency two sets of maps having different baselines and grading functions were produced. The map in Fig. 1 displays the high resolution 1415 MHz map which shows the most detail in the radio emission of the cluster. The major components of the emission in the cluster region have been labelled in Fig. 1. With one exception, the labelling conforms to the convention used in Paper I, with additions where necessary because of the higher resolution at 1415 MHz. The exception is the most northerly feature on the western extended arc; this was labelled *H* in Paper I (Fig. 2 of that paper). In the new 1415 MHz map this feature appears detached from the arc, and we have adopted a modified nomenclature: *H* is the arc itself and *K* is the detached feature.

The optical positions of the galaxies marked in Fig. 1 were determined from the *Palomar Sky Atlas* by Goodson, Guindon, and Bridle using the two-coordinate measuring engine at Queen's University as described by Bridle and Goodson (1977). The standard error of these positions is $\pm 0^s.1$ in right ascension and $\pm 0''.4$ in declination. There is an offset in declination of $0''.6$ between these positions and those measured by Wills (see Paper I), but this offset is of no consequence in what follows. The optical positions together with photographic magnitudes estimated from the blue *Sky Atlas* prints by Valentijn (see Sect. IV) are listed with the radio data in Table 2.

To make accurate spectral comparisons between the 1415 and 610 MHz maps, it is important to compare maps made using closely similar baseline coverage in wavelengths at the two frequencies. Not only is it necessary to omit the larger spacings at 1415 MHz but one must also discard the shortest spacing (36 m) at 610 MHz, as this corresponds to an 18 m baseline at 1415 MHz which is unobtainable using 25 m antennas. Figures 2a and 2b show the low-resolution 1415 MHz map and the appropriate "spectral comparison" 610 MHz map. It is from these two maps that the most accurate spectral information can be deduced.

The 610 MHz map which contains the 36 m spacing was presented in Paper I. Diffuse emission around component *D* is more noticeable in this map since it included the shortest spacing containing nearly all of the data associated with the diffuse emission. Otherwise the differences between the two 610 MHz maps are small.

In Table 2 we have listed the position, flux density at the two frequencies, the 610–1415 MHz spectral index and the approximate angular size for the major components. The definition of the boundary for each component is subjective but precisely the same regions were taken using the maps in Figs. 2a and 2b which have similar resolution and sidelobe properties. The flux density of each component was determined by the following procedure:

1. The zero offset of each map due to the missing short spacings was determined in the vicinity of each source by averaging the intensities on the map where there was no emission. These zero-levels varied somewhat over the cluster region, averaging −0.16 mJy at 610 MHz and −0.09 Jy at 1415 MHz.

2. The intensities, after making the zero-level correction, were summed over the region defined by the component.

3. The intensities in the restoring beam used in the cleaning deconvolution technique were summed to obtain the normalisation for a one Jansky source.

4. The result of step (2) was divided by that of step (3) to obtain the flux density of the component.

5. The estimate of the error in the flux density of a component was obtained by adding in quadrature the following terms: (a) an estimate of systematic errors in the calibration process of 0.05 mJy, (b) half of the average zero offset to allow for the error caused by the variable zero level over the map, and (c) the rms noise error which is listed in Table 1.

The position of an extended radio component was determined from the centre of mass of the intensities combined in step (2) above. Positions for the smaller-diameter (<20″) components were derived by fitting the synthesized beam to the component on the map. Uncertainties in the positions were estimated by combining in quadrature (i) an error derived from the signal-to-noise ratio for the component and (ii) a $0''.5$ systematic error. The 610 MHz data in Table 2 supersede those given in Paper I; the major differences are caused by redefinition of the component boundaries.

The distribution of the linearly polarized intensity at 1415 MHz is shown at 55″ resolution in Fig. 3a. The percentage polarization, superimposed on a radiophotograph of the total intensity of Fig. 2a, is given in Fig. 3b. The 23″ resolution 1415 MHz polarization map was extremely noisy and showed no significant small regions of high percentage polarization. At 610 MHz no polarized emission was detected anywhere in the cluster region.

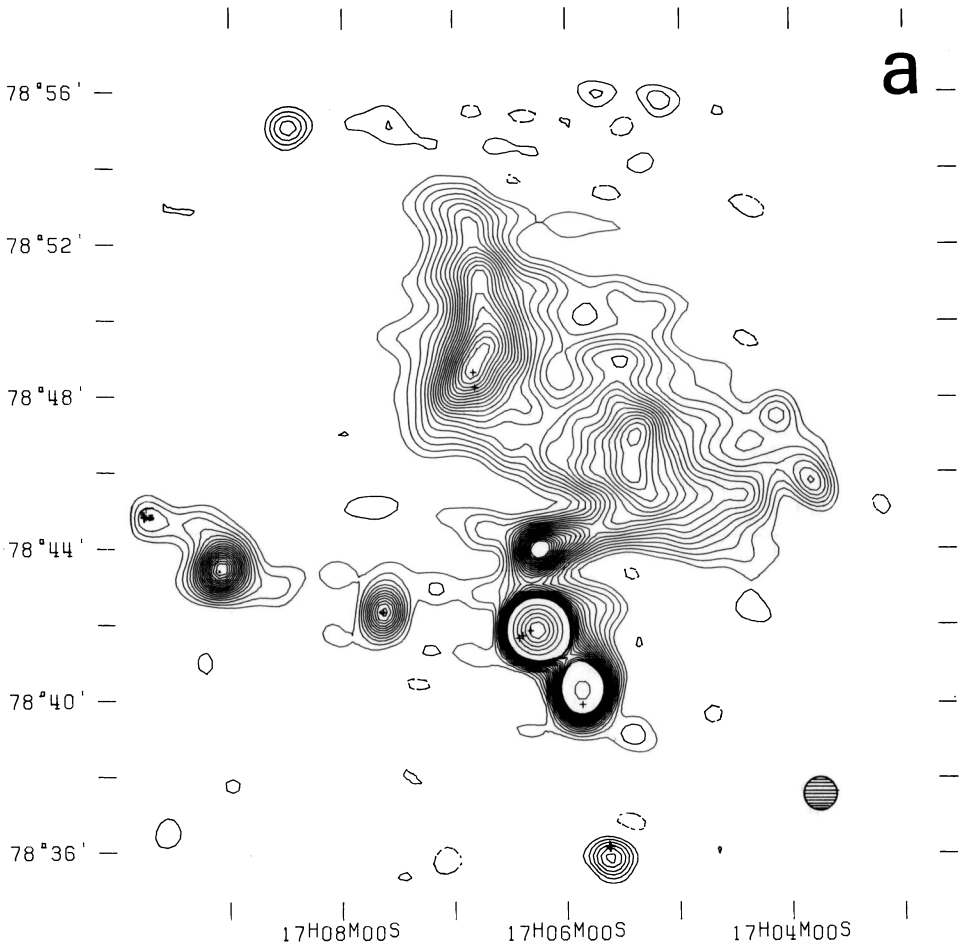

Fig. 2a and b. Radio map of Abell 2256 with 55″ resolution. **a** 1415 MHz with contour levels 0.85–17 in steps of 0.85 mJy per synthesized beam with additional levels of 34–102 in steps of 17 mJy per synthesized beam. **b** 610 MHz with contour levels 2–40 in steps of 2 mJy per synthesized beam with additional levels of 80, 120, 160, 200 mJy per synthesized beam Contour levels at the two frequencies have been adjusted to give the same contour level for emission with a spectral index of 1.0. The shaded ellipse shows the half-power synthesized beam and the small crosses mark the position of some cluster galaxies

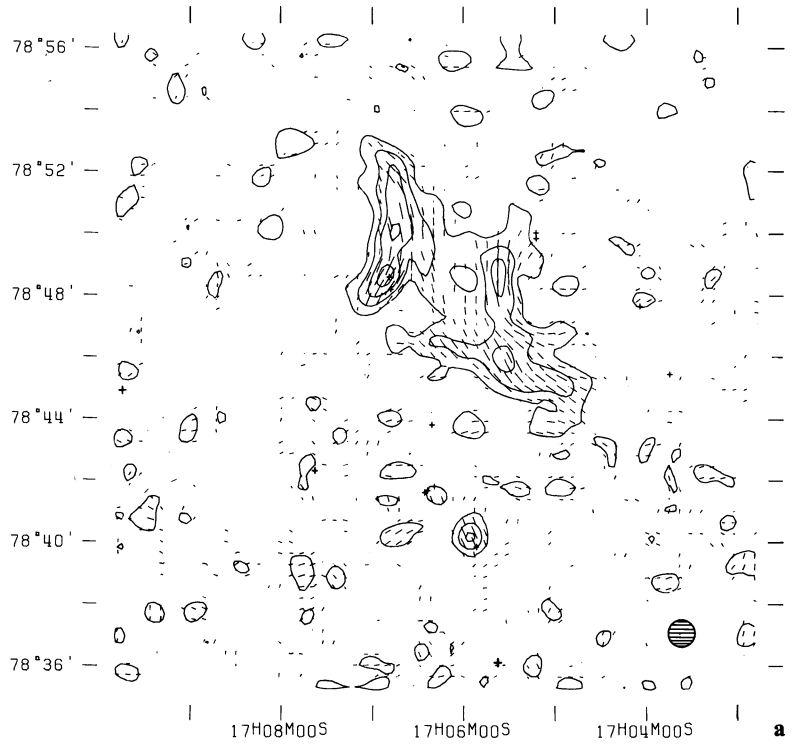

Fig. 3a and b. Distribution of polarized intensity from Abell 2256 at 1415 MHz with 55″ resolution **a** Contour levels of the intensity are at 0.85–3.4 in steps of 0.85 mJy per synthesized beam. The length of each line segment indicates the polarized intensity; the orientation of each line segment is equal to the position angle of the electric vector. **b** Percentage polarization is shown by the contours which are drawn only in regions where the polarization signal is at least four times the rms noise. Dashed regions show upper limits. The contours are superimposed on a radiophotograph of the map in Fig. 2a

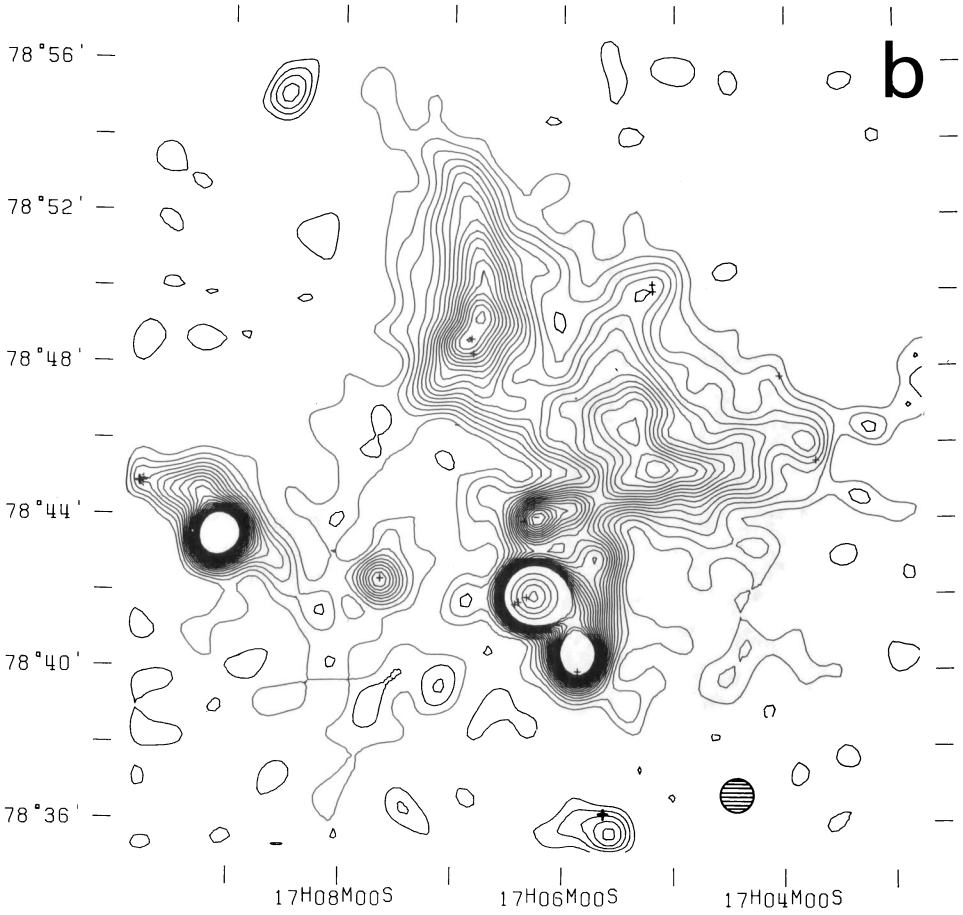

Fig. 2. b

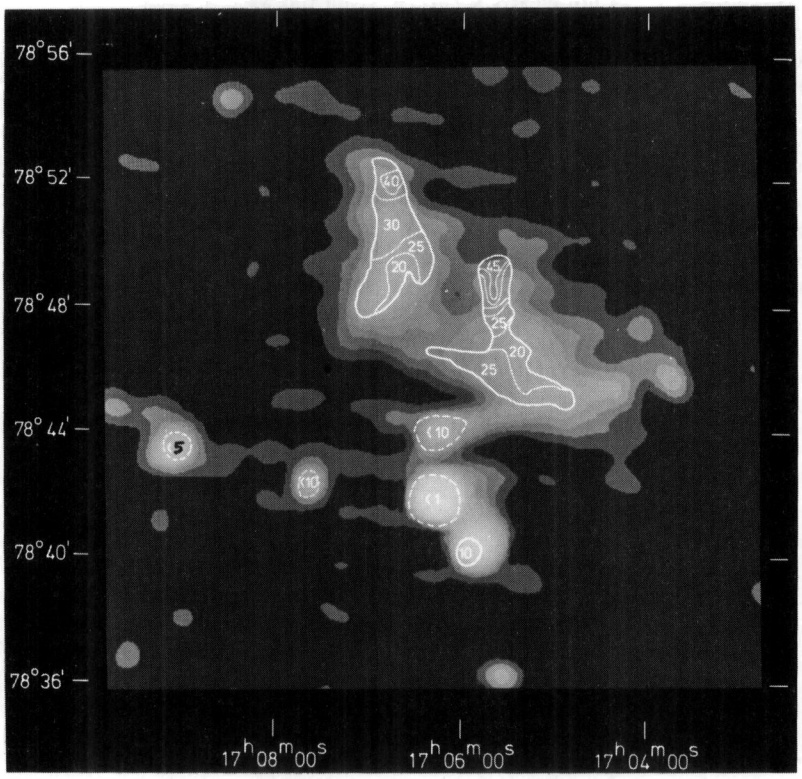

Fig. 3. b

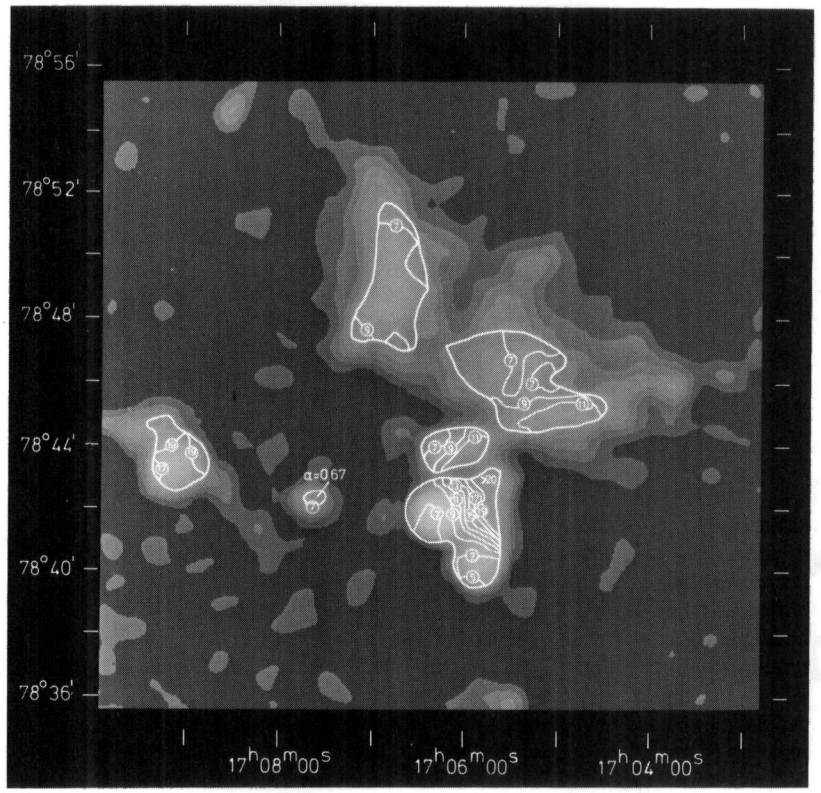

Fig. 4. The spectral-index distribution in Abell 2256 with 55″ resolution. Contour levels of the spectral index (multiplied by 10; i.e., $S \propto \nu^{-1.2}$ would contour at a 12 level) derived from Figs. 2a and 2b. The contours are defined in regions where the total intensity at both 1415 MHz and 610 MHz is greater than 4 times rms noise. The contours have been superimposed on a radiophotograph of the map at 610 MHz in Fig. 2b

Contours of the 610–1415 MHz spectral index distribution are shown in Fig. 4. They are superimposed on a radiophotograph of the 610 MHz map shown in Fig. 2b. A significant source of error in this map is the uncertainty of the variable zero-level depression. From a comparison of the spectral-index distributions generated from the 610 MHz maps, with and without the 36 m spacings, we estimate a relative uncertainty of no more than 0.1 in the spectral index because of the zero-level variations. This should also approximate the absolute uncertainty in the spectral index of the smaller-scale structure in the cluster at any point.

The sum of the emission of the components listed in Table 2 is about 20% less than the total flux density measured by the NRAO 300-ft telescope (Paper I) at 610 and 1415 MHz. Most of the "missing" large-scale structure (angular scale >20′) may be associated with components *G* and *H* in the complex emission to the north of the cluster.

II. The Major Radio Components

a) Definite Head-tail Sources

From the highest-resolution map in Fig. 1, we confirm the suggestion made in Paper I that sources *B* and *C* have a head-tail morphology. Component *A* is known to be a head-tail from higher resolution 2.7 GHz observations at NRAO (Paper I). These conclusions are strengthened by the spectral index distributions across these sources; in both *B* and *C* the spectrum steepens along the tail away from the galaxy (see Fig. 4). Such spectral index distributions are common among head-tail sources. Note that north of *A* and west of *B*, where the tails of these sources are superimposed, the spectral index exceeds 1.7.

The new 1415 MHz map also suggests that component *I* is a head-tail source, from the evidence of its radio contours directly and from the position of a cluster galaxy near the brightest part of the emission at the western end of the component. Component I was not clearly separated from the western extension of component *C*(II) in the 610 MHz maps. Component *M*, which lies near a cluster galaxy about 13′ east of the cluster centre, may also have a head-tail morphology. A contour plot of its 1415 MHz emission is shown in Fig. 5.

b) The Complex Emission to the North of the Cluster Centre

This emission consists of the two diffuse arcs *G* and *H* (Fig. 1). It has a remarkably uniform spectral index of 0.8 ± 0.1 over the entire 1 Mpc by 0.3 Mpc region between 610 MHz and 2695 MHz (Haslam et al., 1978) with the exception of the region near *C*(II) which we interpret as the outer part of the tail associated with *C*. There are no relatively bright subcomponents in these regions which might indicate association of *G* or *H* with individual "active" galaxies although as noted in Paper I there are some cluster members in the area of sky covered by the complex emission.

The percentage polarization (Fig. 3b) is surprisingly uniform across *G* and *H* with an average value of about 20%. The alignment of the electric vectors of the linearly polarized distribution at 1415 MHz (Fig. 3a) suggests that the intergalactic magnetic fields are well ordered in both regions *G* and *H*. The curvature of the electric vectors over *G* and *H* also follows the curvature of the ridges of maximum brightness. The Faraday rotation in these regions is unknown, however, so the true alignment of the magnetic field throughout *G* and *H* cannot yet be determined.

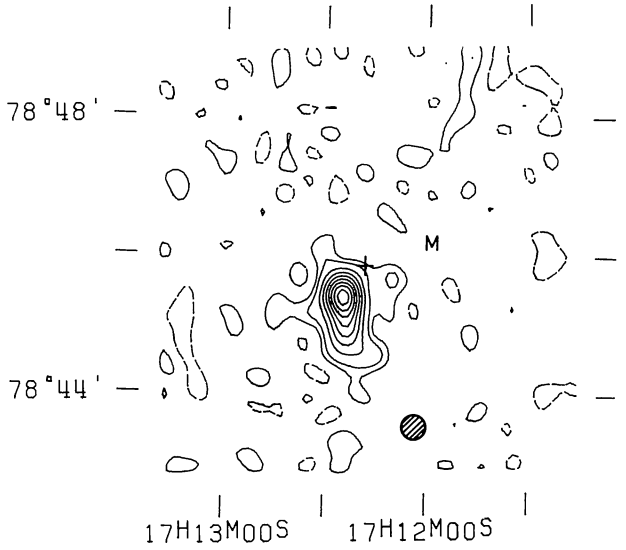

Fig. 5. Radio map of Component *M* at 1415 MHz. Contour levels are at 0.5, 1, 2, 3, 4, 5, 6, 7, 8 mJy per synthesized beam. The cross shows the position of the centre of a galaxy which is a possible optical identification

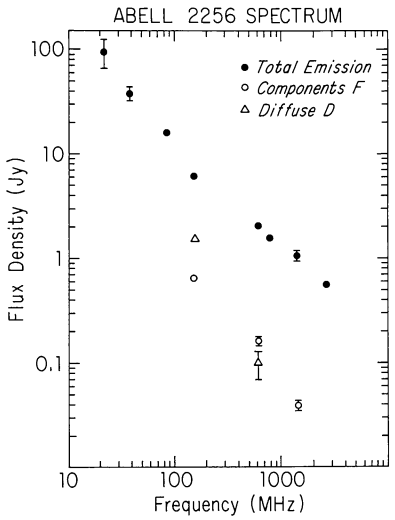

Fig. 6. The Spectrum of Abell 2256. The spectrum between 22 MHz and 2695 MHz for the entire cluster (●), for components $F(I)+F(II)+F(III)$ (○), and for the diffuse emission around *D* (△). Errors are given only when explicitly derived

The nature of this diffuse emission is still unknown. Such uniform spectral and polarization properties are not often seen in extended cluster radio galaxies although similar features have been found in some radio galaxies with radio "jets". Features *G* and *H* could be either a single wide-tailed source whose "head" is presently unrecognizable or two separate sources. In the latter case the small-diameter component *K* might possibly be the "head" of a narrow-tailed source whose tail is feature *H*. Alternatively, *H* might have been produced by leakage of particles from the tail of *C* which may be connected to component *H* in the south-west; if this were true the fact that the spectrum of *H* is flatter than that of *C*(II) would be hard to explain by conventional source models. The location of bright cluster members within *G* suggests that this feature could also be a narrow-tail source.

The homogeneity of spectrum and polarization of arcs *G* and *H* would be less difficult to understand if the linear scale of the complex emission were much smaller than the ~1 Mpc size implied by assuming it to be at the 340 Mpc distance of Abell 2256. The possibility that these features are foreground emission in our galaxy cannot be excluded. The galactic latitude of the field is +32° however and it would be very fortuitous to find such prominent galactic features apparently coincident with a cluster that is definitely rich in extended radio galaxies. For these reasons, as in Paper I, we prefer to interpret all the emission as features associated with Abell 2256, rather than as galactic non-thermal emission.

c) Source F

This source, comprising the components *F*(I), *F*(II), and *F*(III) is especially difficult to relate to conventional source models and common source morphologies:

(i) It has an extremely steep spectrum ($\nu^{-1.7}$) with little variation over the whole source even though it is comprised of parts with differing angular scales. Such steep spectra are exceedingly rare among radio galaxies in general. The steepness of the spectrum and its uniformity across the source are evidence that *F* is indeed a single extended source rather than several unrelated sources.

(ii) No polarization was detected in *F*(II) at 1415 MHz to a low level ($\lesssim 5\%$).

(iii) The overall morphology of *F* is very peculiar. Its *Z*-like appearance shows two-fold rotational symmetry about the bright central region of the source, *F*(II). This component comprises about 60% of the total emission and has a size of ~45″ compared with the overall source size of ~4′. A radio galaxy with such a large overall size would normally be sufficiently close for its optical counterpart to be detectable; from the overall morphology one would expect this to be located under *F*(II) but, as noted in Paper I, no identification candidate can be found there. However, as shown in Fig. 1, there is a cluster galaxy near the eastern extremity of the source and this is a possible (but unconfirmed) identification candidate. If this galaxy could be confirmed as the identification, the entire steep-spectrum region associated with *F* would be an unusual curved "head-tail" structure. In this case the bright unpolarized component *F*(II) might be either a long section of the tail oriented along the line of sight or a section of the tail that was produced by heightened activity of the parent galaxy at some time in the past.

d) The Diffuse Emission around Source D

The region around the unresolved source *D* contains a very diffuse, extended component. This component can be seen most clearly in Fig. 1 of Paper I, in which the 36 m spacing was included, but it is also present in Fig. 2b at 610 MHz and marginally present in Fig. 2a at 1415 MHz. After removing all of the discrete sources in the cluster and correcting for the zero-level offset around the cluster region, the excess in brightness near source *D* is 0.10 ± 0.02 mJy/beam at 610 MHz and 0.02 ± 0.02 mJy/beam at 1415 MHz with a 55″ beam at both frequencies. The angular diameter is uncertain but we estimate it to be about ten arc min centred near the unresolved source *D*. Assuming this angular size the diffuse component contains about 0.1 Jy at 610 MHz and 0.02 Jy at 1415 MHz. Although the error of the flux density is

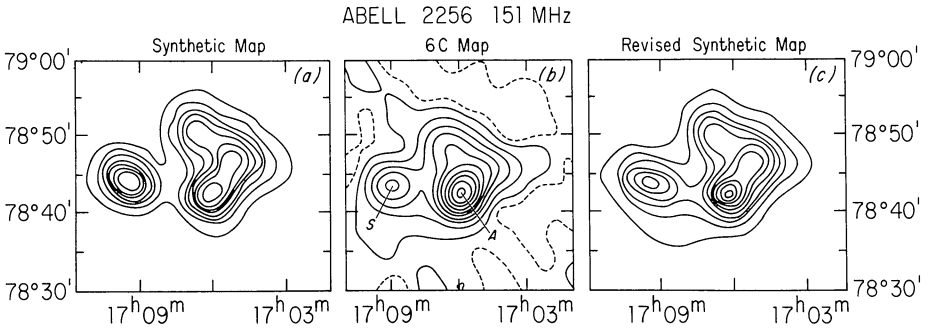

Fig. 7a–c. Synthetic and observed radio maps of Abell 2256 at 151 MHz. The beam size is 4.′6 and the contour interval is 180 mJy per beam with the first positive and negative contour at 90 mJy per beam. The zero contour is omitted and the negative contours are dashed.
a Preliminary synthetic map derived directly from the 610–1415 MHz maps and spectral indices.
b The observed 6 C map at 151 MHz (Masson and Mayer, 1978)
c Revised synthetic map from the 610–1415 MHz maps with the addition of 1.5 Jy in the diffuse component around *D* and downward revision of the flux density of *F*(II) (see text, Sect. III)

uncertain because of the poorly determined radio size, the ratio of the emission at the two frequencies is not and suggests that the diffuse emission around *D* has a spectral index greater than 1.2.

It is notable that in the 610 MHz map made from all of the data, the very steep-spectrum emission associated with source *F* appears to mark the eastern boundary of the diffuse emission, suggesting that the latter may be an extension of source *F*. Source *D* itself has a spectral index of 0.67.

III. The Low-frequency Emission from Abell 2256

The spectrum of the total emission from Abell 2256 between 22.25 and 2695 MHz is shown in Fig. 6 (filled circles). The spectrum steepens below ~100 MHz, implying that at least one component of the radio emission has a spectral index significantly greater than 1.5 (Costain et al., 1972). The angular size and physical scale of this low-frequency excess emission are important parameters for models of the X-ray emission from Abell 2256 (see Introduction). In particular, one might ask: can source *F*, which we have already shown to have an anomalously steep spectrum between 610 and 1415 MHz, be solely responsible for the low-frequency excess? If this were the case, the Baldwin-Scott interpretation of the correlation between the steep spectrum and the X-ray emission would definitely be favoured in this cluster.

To investigate this question we compared our data with the 151 MHz (6 C) map of the cluster (Masson and Mayer, 1978). Figure 7 shows (a) a synthetic 151 MHz map at the 6 C resolution (4.′2) produced by extrapolating our 610 Map to 151 MHz and (b) the actual 6 C map. The synthetic map was constructed on the assumption that for each component the spectrum between 610 and 151 MHz continues the power law defined by our data between 1415 and 610 MHz. *The extrapolation was not made for the weak diffuse emission around source D* as this emission was very faint at 1415 MHz (see Sect. IId).

Although there is general agreement between the synthetic and observed maps in Figs. 7a and 7b, there are two differences which have important consequences for the origin of the low-frequency excess. First, the peak denoted '*S*' by Masson and Mayer is weaker in the observed map than the extrapolation predicts. Second, the minimum between peaks '*S*' and '*A*' is much shallower in the observed 6 C map than in the synthetic 151 MHz map. This is consistent with the fact that Masson and Mayer derive equivalent Gaussian diameters for the region around their peak '*S*' which are significantly larger than the size of our source *F*.

The emission missing from synthetic map (a) between peaks '*S*' and '*A*' is in the region of our discrete source *D*. It is very unlikely however that the contribution of source *D* itself has been significantly underestimated at 151 MHz, as its 610–1415 MHz spectral index of 0.65 is well defined by our data. *Inclusion of a substantial 151-*MHz *flux density in a diffuse component around source D can however bring the observed and synthetic 151-*MHz *maps into good agreement in the region between peaks 'S' and 'A'.*

To determine the possible contribution of such a diffuse component at 151 MHz we included a Gaussian (10′ FWHM) component centred on 17^h08^m, 78°42′ in our synthetic map and optimized its flux density to give best agreement with the observed 151 MHz map between peaks '*S*' and '*A*'. The result gives a flux density of 1.5 Jy for the additional diffuse component and a 151–610 MHz spectral index of ~1.8 if it is identified with the diffuse emission around '*D*'. Such a spectral index would be consistent with our 610 and 1415 MHz maps.

The discrepancy between the peak of '*S*' in the initial synthetic map (Fig. 7a) and the lower peak actually observed by Masson and Mayer at 151 MHz is enhanced by the inclusion of this extra diffuse component. This discrepancy can be removed if source *F*(II) has a 151 MHz flux density of only ~0.65 Jy rather than the extrapolated 1.04 Jy used in constructing Fig. 7a. This would require the spectral index of *F*(II) to decrease to ~1.35 below 610 MHz from the 1.70±0.17 derived from our 610–1415 MHz comparison. Figure 7c shows a revised synthetic map in which we have 1. included 1.5 Jy in a 9′ component centred at 17^h08^m, 78°12′ and 2. decreased the flux density of *F*(II) from 1.04 to 0.65 Jy. *Figure 7c is in much better agreement with the observed* 6 C *map than is the extrapolation based only on the more compact components.* Both synthetic maps contain more emission than the 6 C map in the region between components *H* and *C*(III), but this discrepancy is of no consequence in what follows.

Figure 6 (open symbols) shows the spectra for the diffuse emission around '*D*' and for the components comprising '*F*' which produced the successful synthetic map in Fig. 7c. With

Table 3. Integral bivariate radio luminosity function for E and S0 galaxies

$\log_{10}(P_{1415})_o$ (w Hz^{-1})	Fraction of galaxies with $P_{1415} > (P_{1415})_o$			
	$-23.2 < M_p \leq -22.2$		$-22.2 < M_p \leq 21.2$	
	Abell 2256	Comparison Sample+	Abell 2256	Comparison Sample+
24.8	0/3 = 0.0	0.10	0/38 = 0.0	0.016
24.4	1/3 = 0.3	0.16	1/38 = 0.03	0.03
24.0	1/3 = 0.3	0.21	3/38 = 0.08	0.05
23.6	1/3 = 0.3	0.27	4/38 = 0.11	0.08
23.2	1/3 = 0.3	0.32	6/38 = 0.16	0.11
22.8	1/3 = 0.3	0.41	9/38 = 0.24	0.15

these parameters, the diffuse emission around source '*D*' may contribute the major fraction of the total decametric emission from Abell 2256 if its spectrum remains steep at frequencies below 150 MHz.

Unfortunately, the uncertainties in the above 151/610 MHz comparison are difficult to quantify without more accurate knowledge of the beamshape of the 6 C instrument. However, we conclude that it was clearly premature of Masson and Mayer (1978) to rule out a significant contribution to the low-frequency excess from a diffuse halo. Higher-resolution measurements of Abell 2256 at 151 MHz and at lower frequencies are essential to clarify the situation, and thus to provide a definitive test for the different models of the steep-spectrum emission from this cluster. At present, it is possible that Abell 2256 contains both a steep-spectrum localised source (*F*) as expected on the Baldwin-Scott picture and a steep-spectrum diffuse region (around *D*) as expected on the inverse Compton picture.

IV. Discussion

Our 1415 MHz map shows four definite head-tail galaxies (*A*, *B*, *C*, *I*) and four head-tail candidates (*F*, *G*, *H*, *M*). This is an anomalously large number in one cluster. About 15 Abell clusters closer than Abell 2256 have been mapped by the WSRT with comparable sensitivity and in none except Perseus have more than 2 head-tail galaxies or candidates been detected. In Perseus (e.g. Gisler and Miley, 1979) three head-tails are known, but the weakest of these would not have been recognized as a tailed source at the distance of Abell 2256. Three tailed radio galaxies have also been found in the Hercules supercluster (Valentijn, 1978), but this consists of three Abell clusters each having comparable volume to Abell 2256.

There is no evidence that the apparently large number of head-tail radio sources in Abell 2256 is connected with heightened activity of galaxies in this cluster. Table 3 gives our integral bivariate radio luminosity function (RLF) (Auriemma et al., 1977) which we derive for elliptical and S0 galaxies in Abell 2256 within 11'.5 of the radio field centre. The denominator in each fraction is the total number of galaxies in the given magnitude range which could have been detected above the given radio luminosity and the numerator is the number we actually detected. Our RLF was obtained under the same assumptions and in a similar manner to that of Auriemma et al. (1977) who derived the RLF of a large sample of E and S0 galaxies. There is no significant difference between our RLF for Abell 2256 and the general RLF given by Auriemma et al., nor does the optical luminosity function of Abell 2256 differ significantly from that of other clusters studied by Oemler (1974).

It therefore seems likely that the excess of head-tail galaxies in Abell 2256 should be attributed to unusual properties of the intergalactic environment in this cluster. In most models of head-tail sources (e.g. Miley et al., 1972; Jaffe and Perola, 1973; Pacholczyk and Scott, 1976) the radio tails are viewed as trails produced by active galaxies as they move through an intergalactic medium. Thus the density of the intracluster medium and the relative speeds of the parent galaxies both play key roles in producing tailed sources.

We note that the orientations of the head-tail sources in this cluster are essentially random relative to the cluster centre; this favours head-tail models in which the tails are extended by the motion of their galaxies rather than by buoyant propulsion in the cluster gravitational field, in agreement with the results of Guindon (1978) for head-tails in different clusters.

The radial velocity dispersion for the galaxies in Abell 2256 (1274^{+229}_{-280} km s^{-1}, Faber and Dressler, 1976; Hintzen et al., 1977) is relatively high and the powerful X-ray emission that is observed (Kellogg and Murray, 1974; Mushotsky et al., 1978) could be indicative of a hot dense intracluster medium. There are therefore good reasons for believing that the environment of Abell 2256 may be unusually conducive to the formation of radio galaxies with head-tail morphology.

Some physical parameters pertaining to the radio galaxies in Abell 2256 are given in Table 4. In column 1 we give the 1415 MHz luminosities and in column 2 the magnetic field strengths corresponding to the equipartition energy condition. (In applying this condition we have integrated the radio spectra between 10^7 and 10^{10} Hz and have taken the electron and proton energy densities to be equal.) Many assumptions are always inherent in deriving the equipartition parameters. In the case of Abell 2256 the radio sources are all located at approximately the same distance, so uncertainties in the cluster distance do not affect comparisons between different sources. Also, it may be reasonable to assume that, although its absolute value is uncertain, the electron-proton energy density ratio is constant from source to source. However, since the filling factor of the radiation, the frequency

Table 4. Some intrinsic parameters for the major radio components of Abell 2256[1]

Comp.	1415 MHz Luminosity (10^{23} w Hz^{-1})	"Bolometric"[2] Luminosity (10^{40} erg)	Equipartition[3] mag. field (10^{-6} g)	$n_e T$ (10^3 K cm^{-3})	Linear Extent (kpc)
A	22.0	16	15.		22
B	8.5	6.1	1.9	2.2	180
C(i)	5.4	4.8	1.9		}570
C(ii)	6.6	6.5	1.6	1.4	
D	1.5	1.0	>10		<7
D[4] (diff)	<7	{16 4.9	1.9 0.3	2 0.05}	(600)
E	0.6	0.42	>6		<7
F(i)	0.9	2.8	>5		60
F(ii)	3.1	19	4.7	13	66
F(iii)	1.5	6.4	>7		44
G	25	18	2.5	3.5	150
H	23	17	1.3	0.9	350
I	1.4	1.6	2.9		148
J	0.9	0.72	>10		<7
K	0.7	0.86	>12		<7
L	0.7	0.58	>9		<7
M	1.7	1.2	>3	>4	83

(1) Assuming distance of 340 Mpc (H_o = 50 km s^{-1} Mpc^{-1}).

(2) Assuming radiation between 10^7 and 10^{10} Hz with straight spectrum.

(3) Assuming cylindrical symmetry, equal energies in protons and electrons and radiation and filling factor of unity.

(4) For component D we give two extreme values calculated from the 610 MHz measurements. The upper corresponds to cylindrical symmetry with a spectrum having α = 1.8 extending from 10^6 to 10^{11} MHz. The lower corresponds to spherical symmetry with a spectrum having α = 0.8 extending from 10^7 to 10^{10} MHz.

range over which the radio spectra extend and the effects of projection are all unknown, we caution against deriving conclusions which depend on the detailed validity of these equipartition parameters.

The equipartition condition is most likely to hold in the most relaxed components of the map; for these components we give in column 4 of Table 4, the product n_eT of density and temperature which would be necessary to balance their minimum internal energies by external thermal pressure. Taking the X-ray size of 16′ (Kellogg and Murray, 1974) together with the observed X-ray luminosity and spectral index (Mushotsky et al., 1978) gives $n_eT = 16\ 10^4$ K cm^{-3} on a thermal-bremsstrahlung model. The parameters derived from our radio data for the central regions of the cluster are therefore consistent with confinement of these sources with a hot gas which produces bremsstrahlung X-rays. The differences among the values of n_eT in column 4 of Table 4 may reflect either actual variations in the properties of the intracluster medium in Abell 2256 or erroneous assumptions made in the derivation of the equipartition parameters.

Because of its uncertain spectrum and angular size the parameters of the diffuse component around source *D* are especially subject to error. We note however that the lower value derived for the equipartition field strength of this component is close to the value required for it to produce the X-ray luminosity of Abell 2256 by inverse Compton emission. That model would require a magnetic field strength throughout the diffuse component of ~0.1 microgauss combined with a spectral index of $\alpha = 1.8$ extending to a frequency of 0.17 MHz. Although recent observations of the "iron line" in several other clusters favour a thermal bremsstrahlung origin for their X-ray emission, it is therefore possible that a significant part of the X-radiation observed from Abell 2256 might be produced by the inverse Compton mechanism.

Our results indicate that the history of relativistic particles ejected from the radio galaxies in this cluster has been distinctly different in different parts of the cluster; in the head-tail structures *B* and *C* there is strong evidence for spectral steepening away from the parent galaxies, while in the arcs *G* and *H*, which are of linear extent comparable to *B* and *C*, no spectral variations are found. We also find evidence for *both* well-confined steep-spectrum emission (source *F*) *and* diffuse, possibly steep-spectrum emission, in the south-eastern part of the cluster. This rich variety of behaviour of the particles ejected into a single cluster shows that it would clearly be premature to attempt to describe cluster radio sources by a single model of confinement and evolution.

Because of its large extent and remarkable complexity we will ultimately be able to use the radio emission in Abell 2256 to probe

a large fraction of this cluster's volume. Comparison of the radio data presented here with the high-resolution X-ray maps that are likely to be available in the near future should result in unique information about the physical conditions in the intracluster environment of Abell 2256. Of particular importance will be the location and morphology of the extended X-ray emission in relation to the diffuse radio emission around source *D*, with which it would approximately coincide if it were primarily inverse-Compton emission.

Acknowledgements. We acknowledge stimulating discussions with Dr H. E. Ineken and thank our many colleagues at Westerbork, Dwingeloo, and Leiden who facilitate the smooth running of the WSRT and its reduction systems.

The WSRT is operated by The Netherlands Foundation for Radio Astronomy (S.R.Z.M.) with financial assistance from the Dutch Organization for the Advancement of Pure Research (Z.W.O.). This research has been partially supported by grants to AHB from the National Research Council of Canada and from the Advisory Research Committee of Queen's University and to EAV from Z.W.O.

References

Auriemma, C., Perola, G.C., Ekers, R., Fanti, R., Lari, C., Jaffe, W.J., Ulrich, M.H.: 1977, *Astron. Astrophys.* **57**, 41

Baldwin, J.E., Scott, P.F.: 1973, *Monthly Notices Roy. Astron. Soc.* **165**, 259

Bridle, A.H., Fomalont, E.B.: 1976, *Astron. Astrophys.* **52**, 107 (Paper I)

Bridle, A.H., Goodson, R.E.: 1977, *J. Roy. Astron. Soc. Canada* **71**, 238

Brouw, W.N.: 1971, Ph.D. Thesis, University of Leiden

Costain, C.H., Bridle, A.H., Feldman, P.A.: 1972, *Astrophys. J.* **175**, L15

Faber, S.M., Dressler, A.: 1977, *Astron. J.* **82**, 187

Gisler, G., Miley, G.K.: 1979, *Astron. Astrophys.* **76**, 109

Guindon, B.: 1978, *Monthly Notices Roy. Astron. Soc.* **183**, 195

Haslam, C.G.T., Kronberg, P.P., Waldthausen, H., Wielebinski, R., Schallwich, D.: 1978, *Astron. Astrophys. Suppl.* **31**, 99

Hintzen, P., Scott, J.S., Tarenghi, M.: 1977, *Astrophys. J.* **212**, 8

Högbom, J.A.: 1974, *Astron. Astrophys. Suppl.* **15**, 417

Högbom, J., Brouw, W.N.: 1974, *Astron. Astrophys.* **33**, 289

Jaffe, W.J., Perola, G.C.: 1973, *Astron. Astrophys.* **26**, 473

Kellogg, E., Murray, S.: 1974, *Astrophys. J.* **193**, L57

Masson, C.R., Mayer, C.J.: 1978, *Monthly Notices Roy. Astron. Soc.* **185**, 607

Miley, G.K., Perola, G.C., Kruit, P. van der, Laan, H. van der: 1972, *Nature* **237**, 269

Mushotsky, R.F., Serlemitos, P.J., Smith, B.W., Boldt, E.A., Holt, S.S.: 1978, *Astrophys. J.* **225**, 21

Oemler, A.: 1974, *Astrophys. J.* **194**, 1

Pacholczyk, A.G., Scott, J.S.: 1976, *Astrophys. J.* **203**, 313

Serlemitsos, P.J., Smith, B.W., Boldt, E.A., Holt, S.S. Swank, J.H.: 1977, *Astrophys. J.* **211**, L63

Valentijn, E.A.: 1978, Ph.D. Thesis, University of Leiden